https://doi.org/10.5194/egusphere-2026-5029
Preprint. Discussion started: 27 August 2026

Vertical aerosol flux in urban ecosystem: how far can we push Doppler lidar aerosol observations?

Maciej Karasewicz[1], Lucja Janicka[1], Ronny Engelmann[2], Livio Belegante[3], Iwona S. Stachlewska[1]

[1]University of Warsaw, Faculty of Physics, Institute of Geophysics, Pasteura 5, 02-093 Warsaw, Poland
[2]Leibniz Institute for Tropospheric Research (TROPOS), Permoserstraße 15, 04318 Leipzig, Germany
[3] National Institute of Research and Development for Optoelectronics INOE 2000, Atomistilor Street 409, Magurele, Ilfov Romania.

Correspondence to: Iwona S. Stachlewska (Iwona.Stachlewska@fuw.edu.pl)

Abstract. This work presents analysis of Doppler lidar-derived vertical aerosol fluxes in urban ecosystems. Based on long-term multi-seasonal measurements, we characterized the dependence of aerosol flux occurrence frequency, direction of the transport and velocity regime on seasons, diurnal cycle and altitude. To synthesize the results, we introduced the term aerosol flux intensity factor and applied it based on the aerosol flux parameters described above. This constitutes the first data analysis and characterization of vertical aerosol fluxes for an urban environment, based on multi-year (2022 -2024) Doppler lidar data in Warsaw, Poland. For additional data filtering, we used data products from co-located microwave radiometer and disdrometer. The measurements were conducted within the routine observations of the Cloud Observations Network (Cloudnet-ACTRIS) at the Warsaw Observatory Station (WOS), an ACTRIS National Facility operated by the University of Warsaw, located on the roof platform of the Institute of Geophysics, Faculty of Physics, University of Warsaw (IGF UW). We observed that aerosol fluxes are most intense during Spring (MAM), particularly at the lowest altitudes during the midday Well-Mixed Layer presence. Summer and autumn (JJA and SON) represent transition periods between spring and winter (DJF), while in winter the aerosol flux intensity is generally low. Our findings suggest that the seasonal distribution of aerosol flux intensity is strongly asymmetric. After DJF, abrupt changes in vertical transport lead to a rapid intensification of aerosol fluxes over a single seasonal transition, while after spring the intensity decreases gradually. This work contributes to the multi-seasonal characterisation of aerosol flux intensity, providing *a priori* knowledge for aerosol vertical transport in the urban environment, and enhancing atmospheric aerosol optical property assessments, particularly in calculations based on temporal averages. The proposed methodology provides the basis for performing similar analysis at other ecosystems or measurement sites.

1. Introduction

The atmospheric boundary layer (ABL) is the lowest part of the troposphere, containing the majority of the atmospheric aerosols (Stull, 1988; Sorbjan 1989). Aerosols have a significant impact on the radiative transfer (Coakley et al., 1983) and clouds microphysics (Twomey et al., 1977) by altering the scattering and absorption properties of the atmosphere (Haywood and Boucher, 2000), affecting air quality (IPCC, 2023) and ultimately contributing to climate changes (Twomey et al., 1977).

https://doi.org/10.5194/egusphere-2026-5029
Preprint. Discussion started: 27 August 2026

Atmospheric aerosols exhibit significant variability in their properties, such as chemical composition, size distribution, and origin. This variability determines their complex roles in radiative forcing and cloud formation, with important implications for air quality (IPCC, 2021). Long-range transport and vertical distribution of aerosols are important factors for assessing the uncertainty in aerosol radiative forcing (Chen et al., 2023; Chung et al., 2005; Mishra and Shibata 2012), cloud formation (Fridlind et al., 2004) and dispersion of air pollution (Wang et al., 2018). The influence of aerosols on climate varies with altitude (Tian et al., 2017) and their vertical distribution plays a dominant role in this regard (Wang et al., 2018; Sun et al., 2024; Gui et al., 2022). The sources and transport processes of atmospheric aerosols remain difficult to characterize (Kim et al., 2021). Atmospheric aerosols have many possible origins (Janicka et al., 2017; Yang et al., 2020; Janicka et al., 2023; Szczepanik et al., 2023), and can easily be influenced by atmospheric factors such as radiation, humidity, precipitation and temperature, leading to changes in their microphysical and optical properties (Guo et al., 2018). Nevertheless, to travel over long distances aerosols need to be transported to higher altitudes by a vertical air movement. Therefore, resuspension and sedimentation processes play a key role not only in vertical transport but also in horizontal transport, as they lift aerosol particles to altitudes where long-range advection becomes possible. These processes are interconnected: emission and resuspension represent the initial stages of aerosol transport, while sedimentation and deposition represent the final aspects of the aerosol particle's lifecycle. Within this framework, resuspension and sedimentation in the atmospheric boundary layer are crucial, as they govern vertical distribution, horizontal transport, and overall aerosols lifespan. Therefore, a multi-seasonal characterization of these processes in ABL is justified and worth further investigation across different ecosystems.

Aerosol sedimentation and resuspension, associated with vertical aerosol fluxes, can be studied using the Eddy Covariance (EC) technique with use of in-situ instruments. Vertical aerosol fluxes are defined as the covariance of aerosol mass concentration and vertical air velocity (Järvi et al., 2009). However in-situ instruments are limited in either spatial or temporal resolution, depending on whether the instrumentation is installed on ground-based EC-towers or aircraft. Recent studies demonstrated the application of the remote sensing techniques, such as Doppler lidar measurements, in atmospheric turbulence research at high temporal and spatial resolutions (Engelmann et al., 2008; Dai et al., 2021; Karasewicz et al., 2024; Abril-Gago et al., 2025). Since aerosol fluxes are inherently linked to fluctuations in the backscatter coefficient, these dynamics also directly influence the uncertainty of aerosol optical property assessments, particularly in calculations based on temporal averages.

The use of Doppler lidar measurements in combination with the EC technique can extend information to a wider range of altitudes, maintaining continuous temporal observations. The lidar-based EC method utilizes the lidar backscatter coefficient as an alternative for aerosol mass concentration and lidar-derived vertical velocity at different altitudes (Engelmann et al., 2008). Thus, remote measurements of vertical aerosol fluxes and their characterization across full height of ABL are possible. Additional support from other remote sensing instruments can further expand the qualitative analysis of vertical transport characteristics.

This paper presents the very first analysis and characterization of vertical aerosol fluxes in an urban environment based on multi-year (2022 -2024) Doppler lidar data from Warsaw, Poland. The main instrumentation used in this study was the Doppler

https://doi.org/10.5194/egusphere-2026-5029
Preprint. Discussion started: 27 August 2026

lidar system (StreamLine XR, Halo Photonics) installed on the roof platform of the Warsaw Observatory Station (WOS), ACTRIS National Facility, located at the Institute of Geophysics, Faculty of Physics of the University of Warsaw (IGF UW). Additionally, data products from co-located microwave radiometer and disdrometer were used to improve the results.

This paper is structured as follows: a description of the measurement sites and instrumentation is presented in Section 2. Sections 3 and 4 describe the methodology and data analysis, respectively, while section 5 summarizes the findings and discusses future perspectives.

2. Experimental Site and Instrumentation

The Warsaw Observatory Station (WOS; 52°12′ N, 20.°58′ E; 112 m a.s.l.) run by the Remote Sensing Laboratory (RS-Lab) at the Institute of Geophysics, Faculty of Physics of the University of Warsaw operates as part of the Aerosol, Clouds and Trace Gases Research Infrastructure (ACTRIS-ERIC) and ACTRIS-PL. The site is an ACTRIS National Facility. The exact location of the station is presented in Fig. 1.

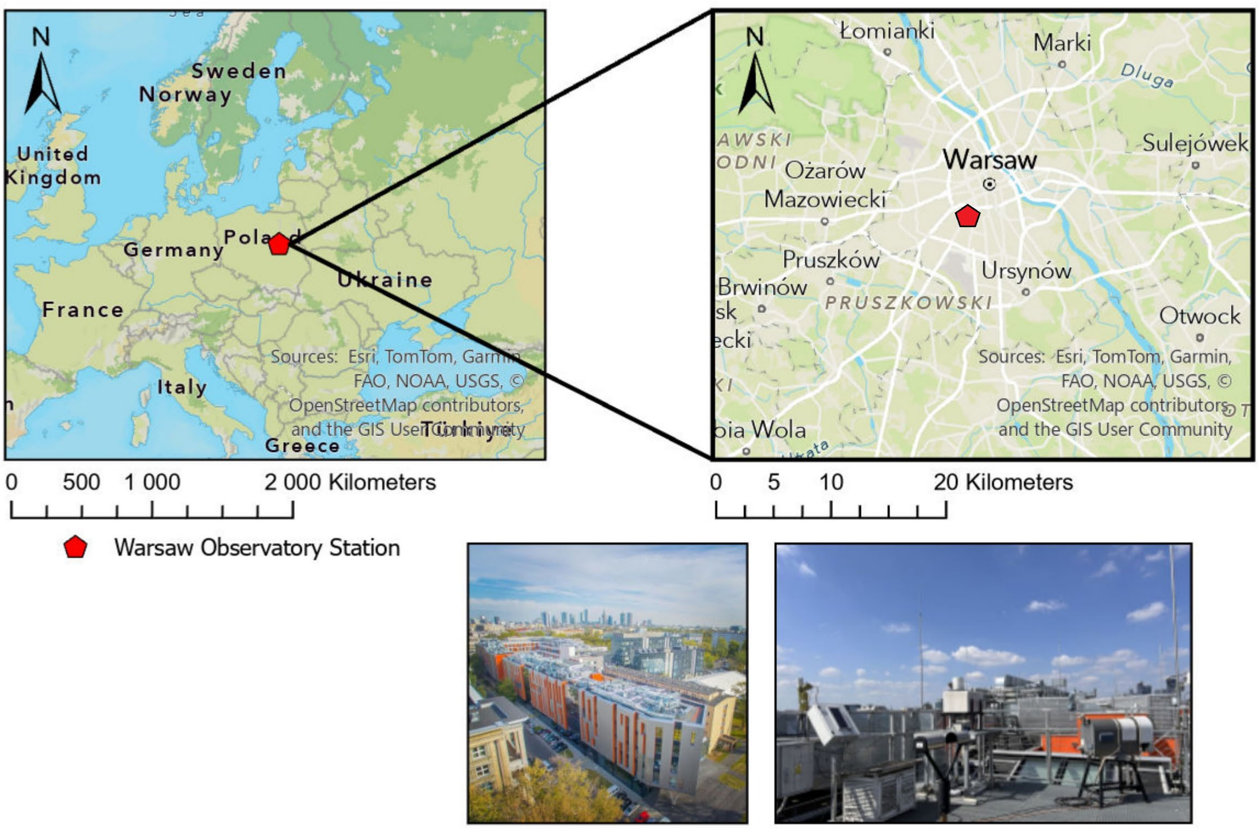

Figure 1: Location of the Warsaw Observatory Station (WOS) - ACTRIS-ERIC National Facility. Doppler lidar, microwave radiometer and disdrometer used in our study are installed on the roof platform of the Institute of Geophysics, Faculty of Physics, University of Warsaw (IGF UW) in the centre of this major urban Polish agglomeration. Sources of Maps: Esri, TomTom, Garmin, FAO, NOAA, USGS, OpenStreetMap contributors, and the GIS user community | Powered by Esri. Source of photograph: www.igf.fuw.edu.pl , author: Marcin Polkowski (left), Maciej Karasewicz (right).

https://doi.org/10.5194/egusphere-2026-5029
Preprint. Discussion started: 27 August 2026

The co-located Doppler lidar, microwave radiometer and disdrometer measurements are a part of the Cloud Observations Network (Cloudnet-ACTRIS) routine observations. The three instruments operate continuously, providing data at high temporal resolution. The Doppler Lidar and microwave radiometer provide high spatial resolution data as well. Each instrument is described below.

StreamLine XR (Halo Photonics) Doppler lidar system is equipped with a solid-state pulsed laser emitting at 1.5 µm and a heterodyne detector with fiber-optic technology. The instrument operates using a pulse energy of 100 µJ; pulse duration of 200 ns and a pulse repetition rate of 10 kHz (Karasewicz et al., 2024). A more detailed description of the Doppler lidar system can be found in (Pearson et al., 2009). The lidar signal was recorded continuously in vertical stare mode, providing products at 30 m spatial and 1 s temporal resolution. The system provides the vertical wind profiles (w) and attenuated backscatter coefficient (β_{att}) components.

Microwave radiometer (HATPRO-G2) operates in two frequency bands at 22–31 and 51–58 GHz, each with seven channels, (Fragkos et al., 2019), with a temporal resolution of 20 s and a height-dependent vertical resolution (Rose et al., 2005). The level-2 products include integrated water vapour, liquid water path, and the vertical profiles of absolute humidity, relative humidity, water vapour, temperature and boundary layer height (Labzovskii et al., 2018). A more detailed description of the instrument can be found in Wang et al. (2020a).

OTT Parsivel^2 HydroMet disdrometer is equipped with a horizontally aligned laser emitter and receiver, connected to the main body by supporting arms. The laser beam power is converted into an electrical signal by a photodiode, and the signal is attenuated by any hydrometeor or other object passing through the beam field (Chinchella et al., 2020).

Since the spatial and temporal resolution of the data provided by each instrument differ, interpolation to common resolutions was necessary. All data products were interpolated to 30 mn temporal and also to 30 m spatial intervals in case of microwave radiometer.

3. Methodology

The complete datasets, consisting of 3 years (2022 -2024) of co-located Doppler lidar, microwave radiometer and disdrometer measurements have been analyzed.

To prepare the data for further analyses, the raw Doppler lidar data was first background-corrected (Manninen et al., 2016; Vakkari et al., 2019) and then filtered using a signal-to-noise ratio threshold SNR = 1.006 (Manninen et al., 2016), resulting in attenuated backscatter coefficient (β_{att}) and vertical velocity products (w) at 1 s temporal and 30 m spatial resolution.

For the calculations of aerosol fluxes, the quasi particle backscatter coefficient ($^{quasi}\beta_p$) and vertical velocity (w) from the Doppler lidar measurements have been used. The $^{quasi}\beta_p$ parameter approximates the particle backscatter coefficient (β_p) and can be obtained at high temporal resolution from the Doppler lidar-derived β_{att} (Wang et al., 2020a; Baars et al., 2017). Aerosol fluxes were computed using an in-house algorithm developed at IGF UW (Ortiz-Amezcua, 2023). The vertical velocity profiles were grouped in 30 mn time intervals, and the recorded signal was decomposed into the mean and fluctuating components.

https://doi.org/10.5194/egusphere-2026-5029
Preprint. Discussion started: 27 August 2026

The detrending process used to isolate the fluctuating component was performed using a linear method. The aerosol vertical fluxes were calculated as a 30 mn means of the covariances between ${}^{quasi}\beta_p$ and w.

The aerosol flux velocity, representing the vertical transport exchange of aerosol particles due to the turbulence movement, is defined as:

$$v_f = \frac{\overline{\beta_p^{quasi}{}' w'}}{\overline{\beta_p^{quasi}}} \quad (1)$$

where positive and negative values correspond to the resuspension and sedimentation of atmospheric aerosols, respectively.

Although a Doppler lidar's attenuated backscatter coefficient depends on turbulence, the total flux values to obtain the flux velocity were divided by the same backscatter. In this way, one could argue that the absolute backscatter doesn't influence, as the result is normalized.

Aerosol flux velocities are classified as resuspension and sedimentation processes, representing upward and downward transport respectively. In a literature these are also referred to as emission/deposition velocities, which we consider imprecise, as these terms are strictly connected with a surface and an air particle exchange, while our results apply to the entire height extent of an ABL. The micrometeorological convention and proper notation are further described in Abril-Gago et al. (2025).

Additionally, cloud filtering was applied using $\beta_{att} > 10^{-5}$ $sr^{-1}m^{-1}$ as a threshold (Manninen et al., 2018). However, no filtering based on the ABLH regime was applied. The algorithm was used not only to profiles within the ABL but also for the upper altitudes up to 1995 m a.g.l.

For data screening of any particle movement associated with precipitation, precipitation flags from the disdrometer were used. If any 30mn time interval within was flagged as precipitation, the entire 30 mn time interval with altitudes up to the cloud base height was classified as so in a spatio-temporal classification.

Relative humidity (*RH*) profiles from the microwave radiometer provided an important reference for assessing hygroscopic growth of aerosol particles, which depends on the type of the particle and *RH* changes (Wonaschütz et al 2013; Tang et al., 2019; Chen et al., 2020). Hygroscopic growth can significantly affect the backscatter signal (Wu et al., 2017), introducing errors in the assessment of ${}^{quasi}\beta_p$ fluctuations. Additionally, hygroscopicity depends on the particle type and *RH* varies with altitude as well as with diurnal and season cycles. Therefore, applying a common threshold across all particles, will lead to a high data loss or inaccurate filtering.

To address this, a cost function for estimating the optimal filtering threshold was applied. Unlike other processing steps, which use fixed thresholds, a fixed *RH* threshold is not feasible due to the lack of information about aerosol type. Since *RH* changes are most pronounced during sunrise and sunset (ABL transition zones) and are closely correlated with ABL evolution (Liu et al., 2012), it was assumed that the filtered data should preserve this temporal variability. The cost function was defined as the sum of the relative standard deviation of the filtered record frequency (normalized to 0-1) and the fraction of remaining data (normalized to 0-1), balancing temporal variability preservation against data loss.

Tests were conducted for the following thresholds: *RH* (50, 60, 70, 75, 80, and 90%) and ΔRH (1, 2, 5, 10%), where *RH* denotes the maximum allowed humidity and ΔRH its maximum allowed change. All parameter combinations were used for the tests.

https://doi.org/10.5194/egusphere-2026-5029
Preprint. Discussion started: 27 August 2026

An additional threshold of *RH* = 75% was introduced to increase the precision of the analysis, as the literature indicates the 70–80% range as a key deliquescing point for many aerosol types (Kuang et al., 2016; Ji et al 2025). The results for the entire dataset are presented in Fig. 2. The best compromise showing the highest variability in filtered data with the lowest data loss was found for the threshold of *RH* > 60% and *ΔRH* > 5% for all seasons at altitudes 75-1995 m a.g.l.
Since we expect these thresholds to vary with season and altitude, as typical *RH* values also vary accordingly, the same cost function was applied separately for each seasons (MAM, JJA, SON, DJF) and altitude intervals (105 - 555, 585 - 1035, 1065 - 1515, 1555 - 1995 m a.g.l.). The optimal parameters for each season and altitude interval are presented in Tab. 1

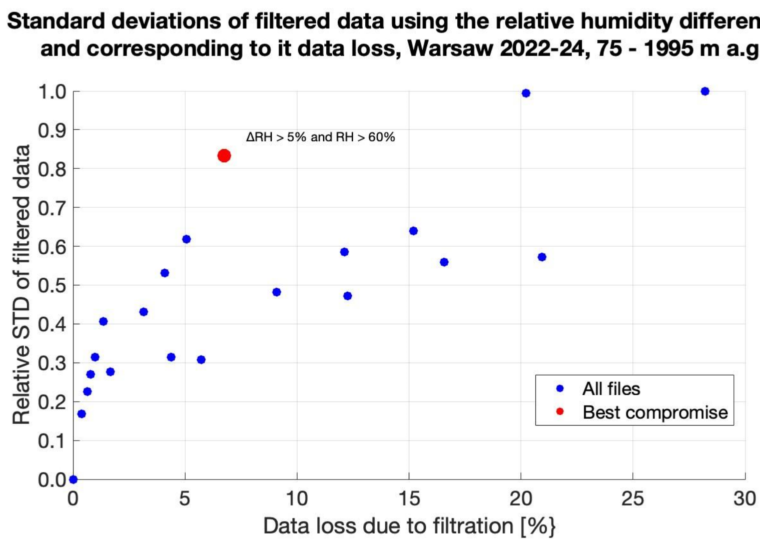

Figure 2. Cost function for the filtering thresholds of *RH* values and its change (*ΔRH)*, applied to the entire dataset.

As shown in Tab. 1, for MAM, JJA, and SON, the *RH* threshold sensitivity decreases with altitude, consistent with the typical decrease of *RH* with altitude. However, the *ΔRH* threshold becomes more restrictive at higher altitudes, likely reflecting the reduced dynamic range of RH changes at those levels. For MAM, this shift is visible just above the lowest altitudes and increases with altitude during JJA up to SON seasons. During DJF, no such altitude-dependent variation was observed in the optimal thresholds. It cannot be ruled out that for the data screened by *RH* data filtering there were no aerosol fluxes present. However these fluctuations could be biased by hygroscopic growth, providing misleading information not in the frequency of flux occurrence but in the distribution of their intensity. Therefore this filtering is fully justified.

Table 1. Relative humidity filtering thresholds with respect to seasons and altitude intervals.

(m a.g.l.)	**MAM**	**JJA**	**SON**	**DJF**
1555 - 1995	ΔRH > 5% and RH > 60%	ΔRH > 5% and RH > 60%	ΔRH > 5% and RH > 60%	ΔRH > 2% and RH > 90%

https://doi.org/10.5194/egusphere-2026-5029
Preprint. Discussion started: 27 August 2026

1065 - 1515	ΔRH > 5% and RH > 60%	ΔRH > 5% and RH > 60%	ΔRH > 1% and RH > 80%	ΔRH > 2% and RH > 90%
585 - 1035	ΔRH > 5% and RH > 60%	ΔRH > 1% and RH > 75%	ΔRH > 2% and RH > 75%	ΔRH > 1% and RH > 90%
105 - 555	ΔRH > 1% and RH > 75%	ΔRH > 1% and RH > 75%	ΔRH > 1% and RH > 80%	ΔRH > 2% and RH > 90%

To investigate whether *RH* data filtering significantly distorted the remaining database, we compared the filtered and retained aerosol flux transport velocities. The remaining dataset was divided into distinct velocity thresholds ($v_f < -5$; $v_f \in [-5, -1)$; $v_f \in$ [-1 0); $v_f \in (0, 1]$; $v_f \in (1,5]$ and $v_f > 5$ cm/s) For each threshold, we calculated its proportion relative to the total flux, stratified the data by altitude and season, and determined the coefficient of determination R^2. The overall R^2 was 0.83. However, for the majority of the results, R^2 exceeded 0.90, except during the winter season. Specifically, high altitudes during winter exhibited a drastic drop in correlation, which substantially reduced the overall R^2 value. Consequently, the results indicate that *RH* data filtering is unlikely to distort the overall statistics, especially for strong aerosol flux events.

In this study, we did not apply data filtering based on stationarity tests. While we acknowledge the importance of these factors, especially in case studies, we assume that the use of extensive, multi-seasonal databases reduces the impact of potential errors to a negligible level. Cases failing to meet stationarity criteria are mostly infrequent (Abril-Gago et al., 2025). To further validate this assumption, we applied stationarity tests to a representative database containing 36 days of measurements from 2024. To avoid seasonal and selection biases, three days from each month (the 1st, 10th, and 20th) were chosen for the tests. If data for the exact day was missing, the previous day was selected instead. We applied the same methodology for the stationarity tests as described in (Abril-Gago et al., 2025). For these tests, covariances were additionally calculated at a 5 mn resolution, and the mean 30 mn values were obtained. These mean values were then compared with the original 30 mn calculated covariances. If the values deviated by more than 60%, the data points were classified as non-stationary, and stationary vice versa. The graphical representation of the frequency of occurrence of stationary conditions is given in Fig. 3.

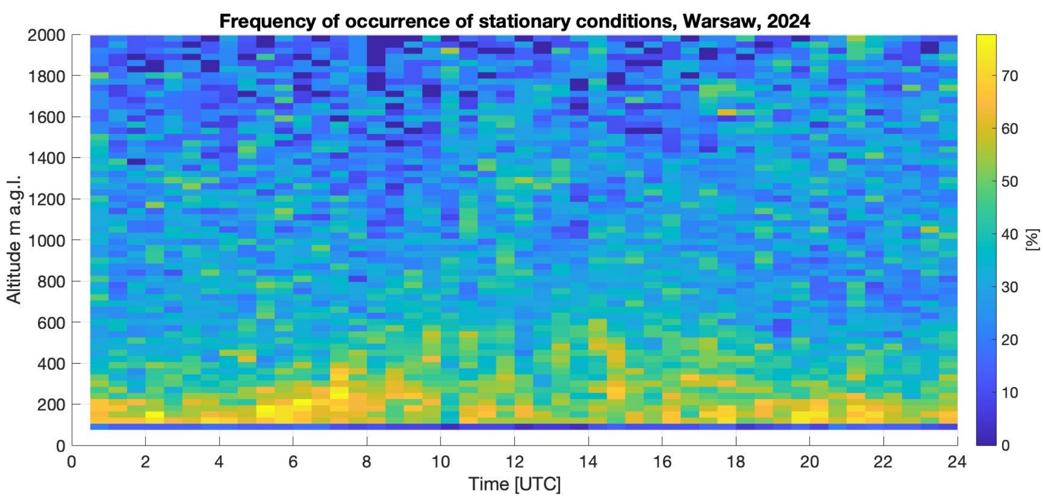

Figure 3. Frequency of occurrence of stationary conditions obtained for the test database from all months of 2024.

https://doi.org/10.5194/egusphere-2026-5029
Preprint. Discussion started: 27 August 2026

Fig. 3 shows a systematic correlation between the frequency of stationarity occurrence, the diurnal cycle, and altitude, indicating that lower altitudes exhibit higher chances of stationary conditions. Similarly, it was shown that during the morning transition and well-mixed layer periods of the diurnal cycle, stationarity can occur even at higher altitudes. To determine whether stationarity tests are necessary for the entire dataset, we compared the stationary and non-stationary aerosol flux transport velocity values, The results are presented on Fig. 4.

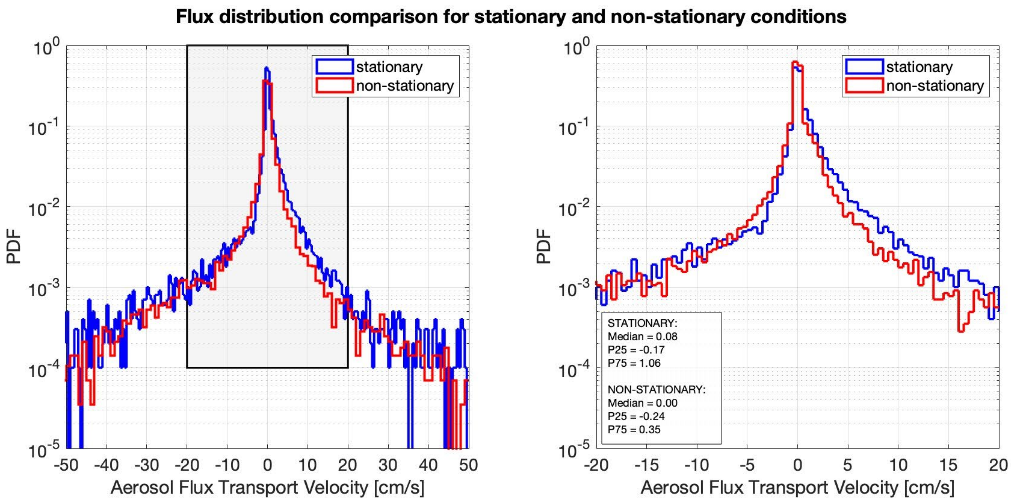

Figure 4. Probability density function of Aerosol flux transport velocity in stationary (blue) and non-stationary (red) conditions. On the right, zoom on the most common velocity ranges.

Overall, the occurrence of stationary conditions within the altitude span of 105 to 1995 m a.g.l. was 30,98 %. Nevertheless, Fig. 4 demonstrates that even under non-stationary conditions, the aerosol flux transport velocity values did not vary substantially from the stationary ones. This can provide a valuable statement that non-stationarity does not change the flux velocity drastically compared to stationary conditions. Therefore, there is no urgent need to apply stationarity tests to the entire dataset, which would result in a drastic reduction of the valid database.

Filtering for advection effects and gravitational waves was also bypassed, as these processes do not represent predominant phenomena in our dataset. Due to the large volume of data, such sporadic events do not significantly alter the findings. A similar approach applies to the estimated sampling error. For a single 30-minute integration period, the random error is indeed substantial, often reaching or exceeding 100% (Engelmann et al., 2008). However, as this study focuses on long-term mean profiles derived from a dataset consisting of 3 years of continuous measurements (approx. 52000 samples per height bin), the error of the mean reduces significantly. Even under a conservative assumption of daily independence (approx. 1000 samples), the resulting statistical uncertainty of the mean flux is approximately 3%. This confirms that the vertical flux profiles are statistically robust and the observed trends are physically meaningful.

https://doi.org/10.5194/egusphere-2026-5029
Preprint. Discussion started: 27 August 2026

The whole methodology chain is presented on Fig. 5.

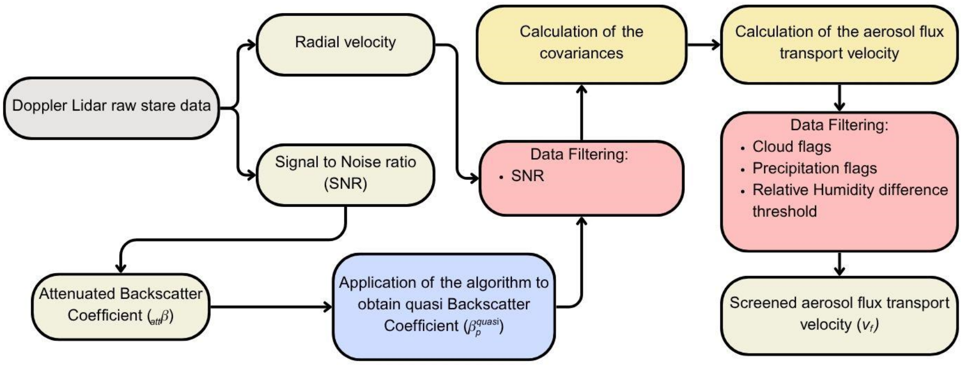

Figure 5. Methodology chain for obtaining the aerosol fluxes transport velocity (resuspension, upward transport, sedimentation, and downward transport). Colour coding: calculation of standard Cloudnet/ACTRIS data products (beige) and additional calculation of the quasi backscatter coefficient (blue) from Doppler lidar. Data filtering (red). Application of the aerosol flux algorithm (yellow).

The results of the aerosol fluxes characterization will be presented with respect to the altitude intervals, seasons and ABL transformation sublayers: Well-Mixed Layer (WML), Transition Layer during sunrise (TLsr) and sunset (TLss), and Nocturnal and Residual Layer (NL+RL). In addition, a full comparison of aerosol flux intensity during nighttime and daytime will be performed. The specific hours (UTC) of each sublayer during the diurnal cycle with respect to the seasons and measurement location were specified in Wang et al. (2020b) and are presented in Tab. 2.

Table 2. Time intervals (UTC) of ABL sublayers per season, after Wang et al. (2020b).

	MAM and SON	JJA	DJF
Daytime	05:00–17:00	04:00–19:00	06:00–15:00
Nighttime	19:00–04:00	20:00–03:00	16:00–06:00
Well-mixed layer (WML)	12:00–16:00	12:00–17:00	12:00–14:00
Transition layer during sunrise (TLsr)	05:00–11:00	03:00–11:00	06:00–11:00
Transition layer during sunset (TLss)	17:00–19:00	16:00–20:00	15:00–16:00
Nocturnal and residual layer (NL + RL)	20:00–04:00	21:00–02:00	17:00–05:00

https://doi.org/10.5194/egusphere-2026-5029
Preprint. Discussion started: 27 August 2026

4. Results

4.1 The frequency of occurrence of aerosol particles

We analyzed three years (2022 -2024) of the Doppler lidar, microwave radiometer and disdrometer observations. The aerosol flux velocities within the ABL were derived at 30 m and 30 mn resolution and grouped by season, altitude and time of the day. After cloud, precipitation and *SNR* filtering, the remaining data was classified as aerosol particle signal. The statistics presented here concern the presence of aerosol particles only. We assume that if particles are present in the atmosphere, their vertical transport also exists. Therefore, to calculate the frequency of occurrence of aerosol fluxes, we used the total signal statistics filtered from the clouds and precipitation. Data filtered out by the *RH* criteria are still included, but in further data analysis, since we are interested only to quantify the presence of the aerosol fluxes, not to characterize their intensity- which was the main purpose of *RH* filtering. The aerosol occurrence frequency, i.e. aerosol flux occurrence frequency is presented in Fig. 6. Colours in Fig. 6 indicate the frequency of aerosol particle presence, with thresholds defined to characterize the dominance or absence of aerosol fluxes with respect to altitude, seasons and diurnal cycle. The presence of aerosol particles is approximately stable throughout the day but varies between seasons. The occurrence of atmospheric aerosols, and consequently of aerosol fluxes occur during MAM and JJA across the entire altitude span, particularly at lowest altitudes. For SON and DJF, aerosols presence decreases with altitude, with DJF showing a higher decrease. The similarity between MAM and JJA is notable, as is the change between JJA and SON. The change in aerosol particle presence is much more abrupt between DJF and MAM, suggesting that the dynamic of ABL growth changes more rapidly during this season's transition.

https://doi.org/10.5194/egusphere-2026-5029
Preprint. Discussion started: 27 August 2026

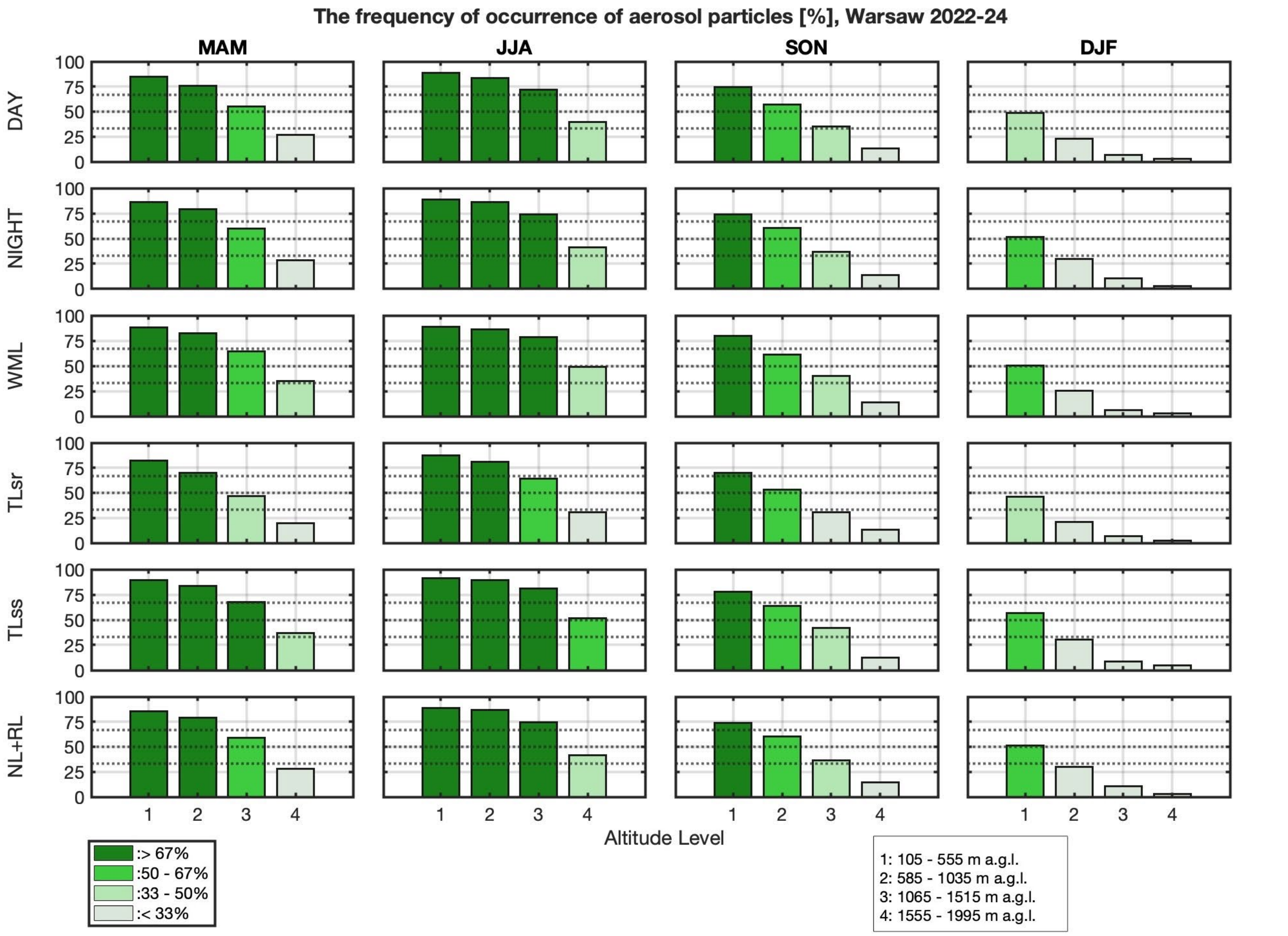

Figure 6. The frequency of occurrence of aerosol particles in %. The dashed lines mark the limits between each threshold. Numbers on the x-axis indicate the altitude levels. The rows names indicate the ABL sublayers and their time intervals according to Tab. 2.

4.2. Aerosol flux characterization

After applying the full methodology, aerosol flux velocity products were obtained. An example for one day of observations under cloud-free conditions is presented in Fig. 7.

https://doi.org/10.5194/egusphere-2026-5029
Preprint. Discussion started: 27 August 2026

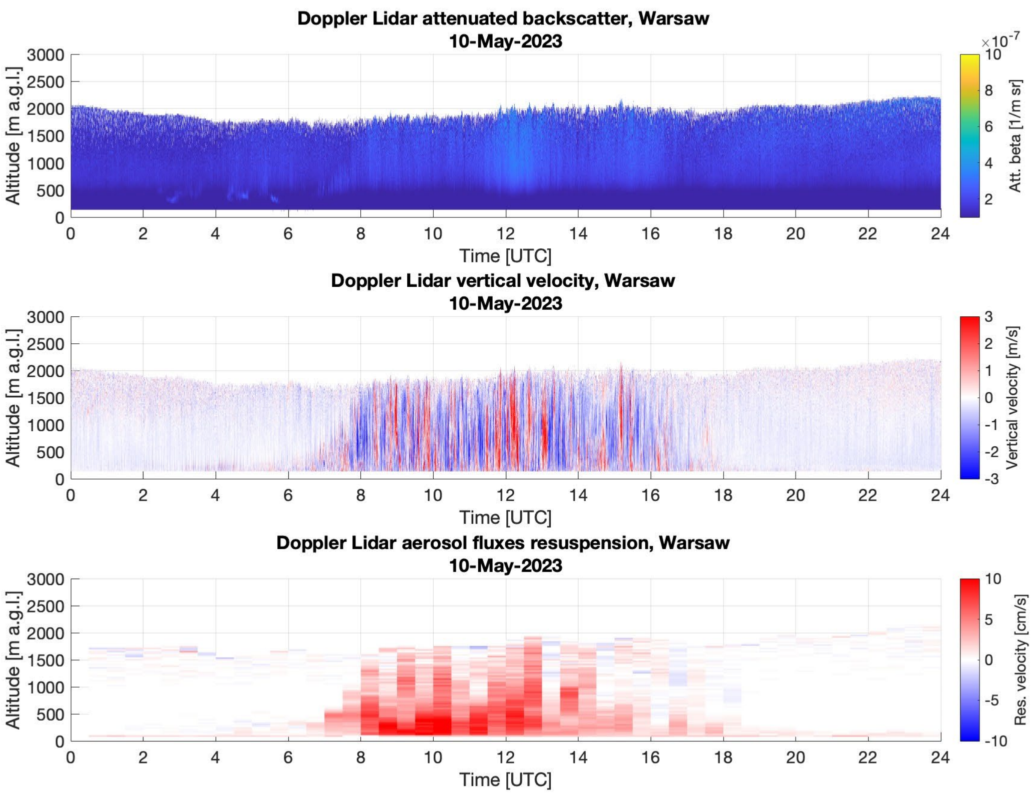

Figure 7. Spatio-temporal representation of attenuated backscatter coefficient, vertical air velocity and aerosol flux transport velocity profiles from 10th of May 2023 at the Warsaw Observatory Station.

The blank region represents the data filtered using the SNR threshold, referred to as a no-signal. The dependence of aerosol flux velocities on diurnal cycle and altitudes is clearly visible. A clear difference can be observed between the direction of vertical air movement (Fig. 7 middle) and that of net aerosol transport (Fig. 7 bottom), demonstrating that these two phenomena are distinct from each other. Fig. 8 shows the median resuspension velocity for all altitudes, together with the 25th and 75th percentiles, to illustrate the seasonal dependencies of aerosol fluxes. The annual cycle of aerosol flux intensification can be divided into two regimes: a period of increased resuspension during the day (MAM and JJA), and a period of much less intense fluxes without significant transport direction (SON and DJF). During MAM and JJA, aerosol flux velocities are higher, particularly for resuspension, while during nighttime only negligible movement is present. During SON and DJF, aerosol fluxes occur with similar frequency during both day and night, but without any dominant direction except in the middle of the day when the dominance of resuspension is slightly marked.

https://doi.org/10.5194/egusphere-2026-5029
Preprint. Discussion started: 27 August 2026

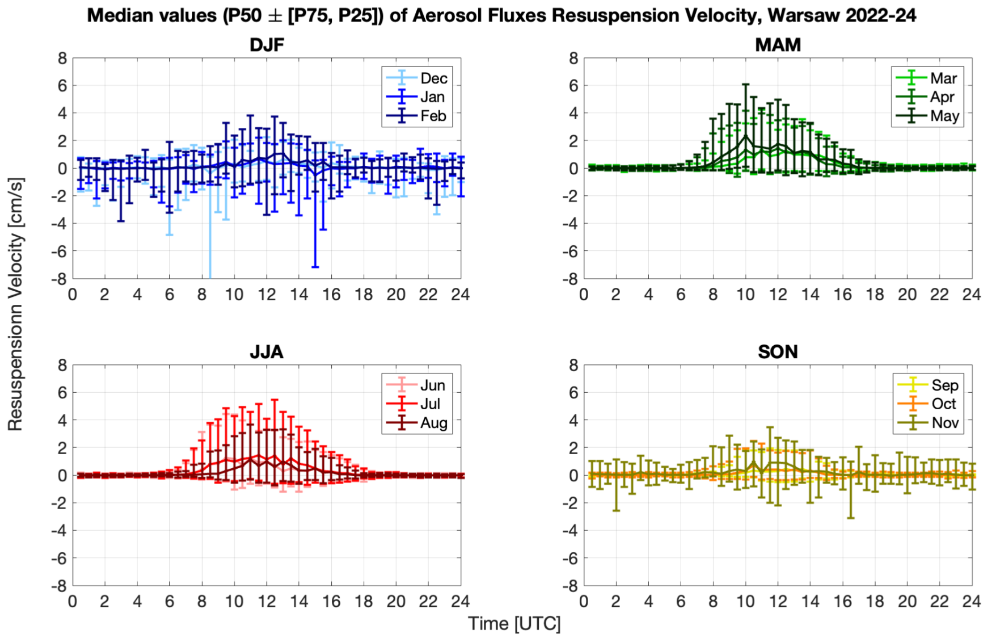

Figure 8. Median diurnal cycle of aerosol flux velocity transport for different seasons (DJF winter, MAM spring, JJA sumer and SON autumn), with the 25th and 75th percentile, based on 3 years of observation (2022 -2024) at the Warsaw Observatory Station.

Since aerosol fluxes are strongly dependent on seasons, altitude and diurnal cycle, further data analysis was conducted on accordingly grouped datasets. Fig. 9 presents the observed frequency of different phenomena occurrences: cloud presence, precipitation, data filtered by the *RH* criteria (according to Tab. 1), no-signal, and the directions and velocities of observed aerosol fluxes during the diurnal cycle. The highest no-signal occurrence is found at higher altitudes, especially during DJF season. Cloud cover and precipitation occur mostly at the lowest altitudes, especially during the DJF season. The highest frequency of *RH* filtered data is observed at lowest altitudes, mostly for MAM, JJA and SON seasons. At the lowest altitudes, particularly during MAM and JJA, the occurrences of *RH*-filtered data differs according to the diurnal cycle. At higher altitudes the several-hour shift of this pattern is observed, indicating humidity transport to higher levels of the atmosphere.

https://doi.org/10.5194/egusphere-2026-5029
Preprint. Discussion started: 27 August 2026

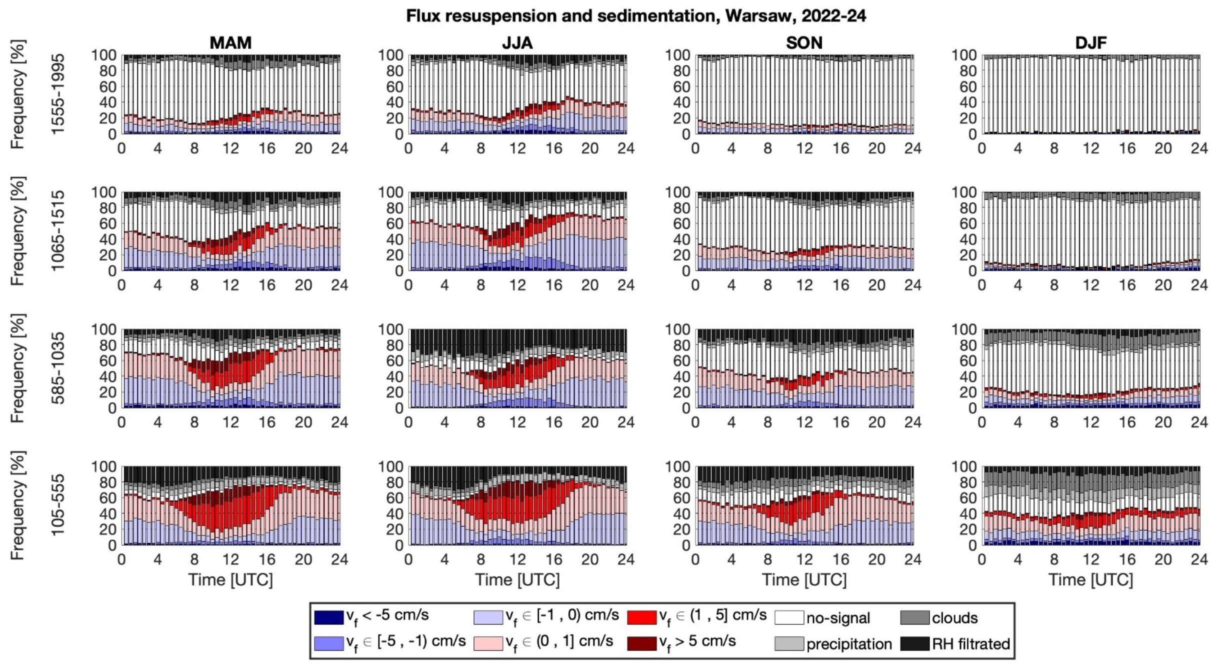

Figure 9. Occurrence frequencies of resuspension and sedimentation flux velocity ranges, *RH*-filtered data, precipitation and cloud presence, and no-signal intervals across different altitudes and seasons based on 3 years of observations (2022-2024) at Warsaw Observatory Station.

Fig. 10 presents the occurrence frequency of aerosol flux direction and velocities, forming the basis for subsequent flux classification. Frequencies are analyzed using velocity thresholds to classify fluxes as significant ($v_f > 1$ or $v_f < -1$ [cm/s]) or less significant ($-1 \leq v_f \leq 1$ [cm/s]) for both resuspension and sedimentation processes. While hygroscopic growth filtering may exclude some genuine aerosol flux occurrences, this data filtering is essential for precise characterization, as hygroscopic effects could distort backscatter signals and introduce errors in covariance and flux velocity estimates.

During spring, summer and autumn seasons (MAM, JJA, SON) clear diurnal variations in aerosol flux velocities within ABL occurred with less significant velocities prevailing at night and significant ones dominating during daytime. However, during winter (DJF), these diurnal differences were largely observed only at the lowest altitudes. For higher altitudes resuspension and sedimentation velocities were mostly classified as significant regardless of the time of day.

https://doi.org/10.5194/egusphere-2026-5029
Preprint. Discussion started: 27 August 2026

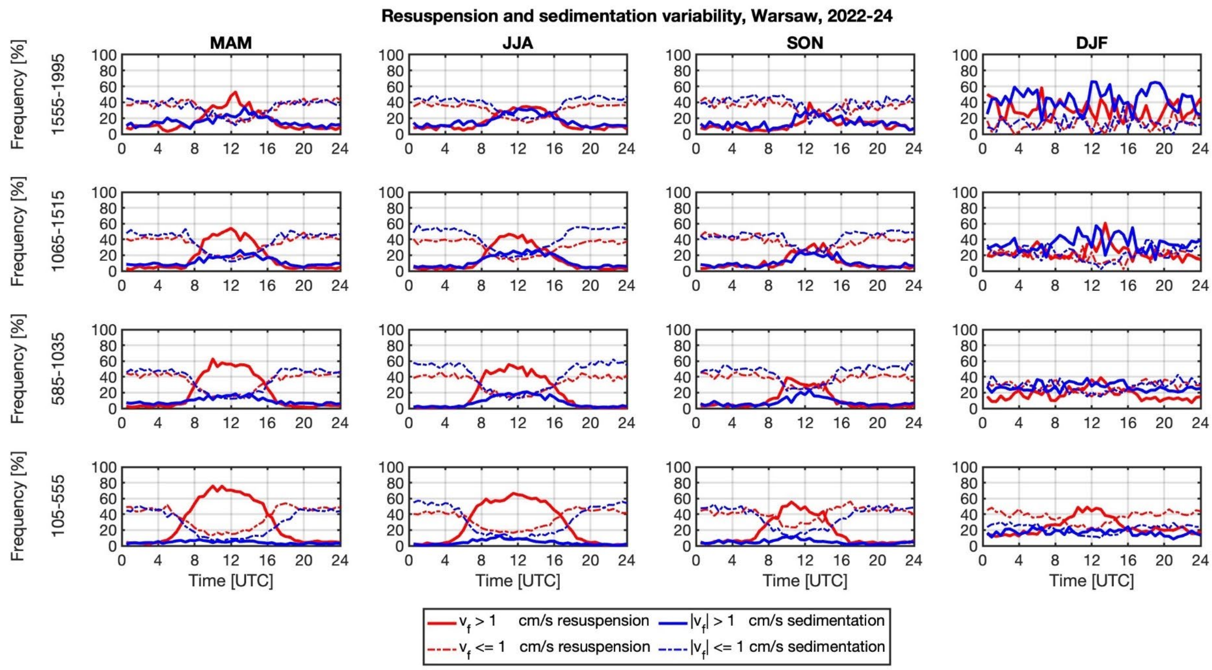

Figure 10. Significant and non-significant flux velocity variability for different altitudes and seasons for 3 years (2022 -2024) of observations in Warsaw Observatory Station.

A clear relationship exists between aerosol fluxes and diurnal cycle, with significant resuspension as a dominant flux type, especially during midday. The analysis reveals stronger resuspension during midday and slower sedimentation and resuspension during nighttime; however, the precise characteristics vary with altitude and season. At the lowest altitudes across all seasons, faster resuspension dominates during midday, with MAM showing the highest occurrence frequency across all altitudes. During MAM nighttime, less significant sedimentation and resuspension can be observed. In JJA, faster resuspension dominates during midday but decreases with altitude transitioning to strong sedimentation at higher levels, while nighttime is characterized by less significant sedimentation occurring more frequently than resuspension. SON exhibits similar nighttime patterns as JJA, whereas during the daytime, fast sedimentation shows comparable occurrence, especially at high altitudes. DJF displays more irregular aerosol flux behaviour, particularly at higher altitudes, potentially due to data filtering effects. At low altitudes in DJF, faster resuspension dominates during midday, while slower resuspension is more common at night; making resuspension the prevailing flux type. Across MAM, JJA, and SON, strong sedimentation frequency increases with altitude, especially during midday. A common feature across all seasons (in DJF limited only to lowest altitudes) is the diurnal transition from slow aerosol fluxes after sunrise to faster ones during daytime, followed again by slower fluxes after sunset.

https://doi.org/10.5194/egusphere-2026-5029
Preprint. Discussion started: 27 August 2026

4.3. Aerosol flux categorization

Based on the obtained data, the following categorization focuses on characterisation of aerosol fluxes according to diurnal transformation within the ABL. Fig. 11 presents the occurrence frequencies of resuspensions and sedimentations processes throughout different parts of the day. Resuspension is classified as the majority process when occurrence exceeds 50% (red). Similarly, sedimentation is marked as majority when occurrence exceeds 50% (blue). Additionally any transport is classified as a dominant one when the direction occurrence exceeds 67%. Similar grouping was conducted for flux velocity regimes and is also represented by Fig. 11. Aerosol flux velocities were classified according to the previously mentioned thresholds as either significant ($v_f > 1$ or $v_f < -1$ [cm/s]) or less significant ($-1 \leq v_f \leq 1$ [cm/s]) for resuspension/sedimentation velocities. The median ratio of the number of occurrences of more significant to less significant velocity fluxes was calculated. Based on the prevailing or dominating aerosol flux velocity, their velocity regimes are shown as median ratios with 25th and 75th percentiles. Percentiles were included to demonstrate the population skewness and possible mode dominance. Values below 1 indicate that fluxes are less significant and relatively slow, while values above 1 indicate that significant, fast fluxes prevail. A median value of 1 would indicate equal occurrence of significant and less-significant fluxes, but no such cases were observed. For broader characterization, the 25th and 75th percentiles were also analyzed. When both the median and the 75th percentile were below 1, less significant slow fluxes dominated. When the median was below 1 but the 75th percentile exceeded 1, this mode was considered merely prevalent. Similarly, when the median exceeded 1 while the 25th percentile was below 1, significant fast fluxes prevailed. When both median and 25th percentile exceeded 1, they were considered dominant. Since the distinction between fast and slow fluxes is more conventional, these terms will be used instead of 'significant' and 'less significant' in subsequent data analysis.

The analysis of the occurrence frequencies of the aerosol transport direction reveals that the dominant sedimentation class (higher than 67%) does not occur throughout the entire dataset. Resuspension predominates at lowest altitudes across all seasons, except during nighttime in JJA and SON. Sedimentation prevails at all altitudes and seasons during nighttime, except the lowest altitudes in MAM and DJF. During the WML, resuspension dominates at low altitudes for all seasons. With increasing altitude, the resuspension frequency decreases towards sedimentation in JJA, SON and DJF. During sunrise, upward fluxes occur at lowest altitudes, with MAM showing the strongest dominance. Similarly to the WML pattern, resuspension share decreases with altitude in JJA, SON and DJF, favoring the sedimentation occurrence. However, this directional shift begins at lower altitudes compared to the WML, while in DJF, resuspension prevails only at the lowest altitudes. The sunset transition layer is predominantly characterized by prevailed sedimentation across all seasons, with resuspension maintaining a majority share only at the lowest altitudes. The nocturnal layer exhibits sedimentation prevalence across all seasons and altitudes, except MAM and DJF where the resuspension is observed at the lowest altitudes.

https://doi.org/10.5194/egusphere-2026-5029
Preprint. Discussion started: 27 August 2026

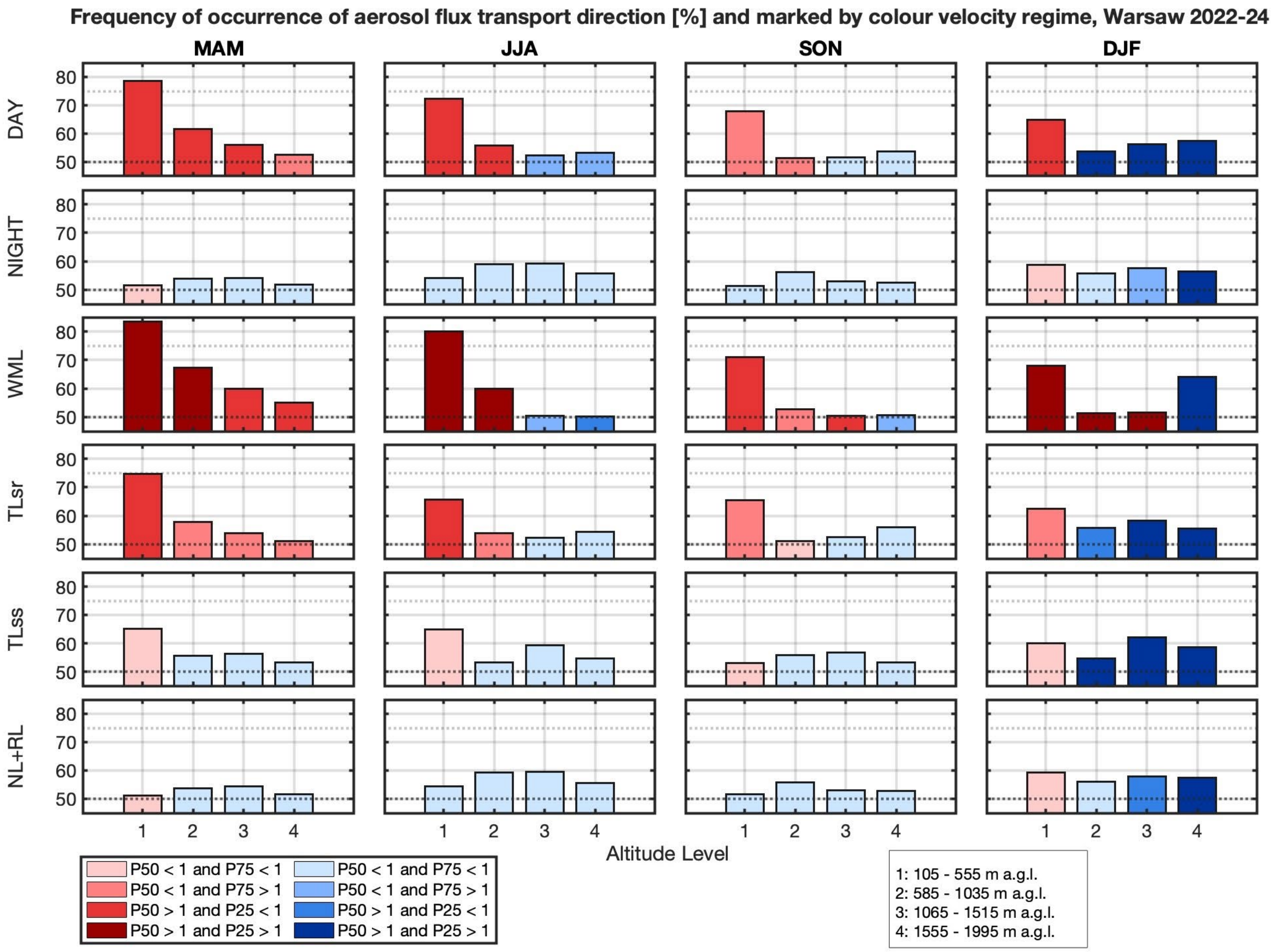

Figure 11. Frequency of occurrence of aerosol flux transport. Colours indicate direction: resuspension (redish) and sedimentation (blueish). When resuspension (or sedimentation) occurrence exceed 50% they are predominant, above 67% they are dominant. The colour tone indicates the values of aerosol flux velocity regime. Numbers on the x-axis indicate the altitude levels. The row names indicate the ABL sublayers and their time intervals according to Tab. 2.

According to the velocity regime, during daytime, particularly for MAM and JJA at lower altitudes, fast resuspension prevails, while JJA shows prevalent slow sedimentation at higher altitudes. SON is characterized by prevalent slow resuspension and dominance of slow sedimentation at low and higher latitudes, respectively, whereas DJF exhibits predominantly fast sedimentation dominance, except at lower altitudes where fast resuspension prevails.

During nighttime, slow sedimentation is dominating at all altitudes for MAM, JJA and SON, except at lowest altitudes in MAM and DJF where the slow resuspension prevails. Additionally, fast sedimentation dominates at higher altitudes during DJF.

https://doi.org/10.5194/egusphere-2026-5029
Preprint. Discussion started: 27 August 2026

During the WML, fast aerosol fluxes dominate, particularly at lower altitudes. Fast resuspensions dominate in MAM, JJA and DJF, while for SON fast resuspension is prevalent. At highest altitudes, JJA shows fast sedimentation and SON exhibits slow sedimentation. DJF demonstrates dominant fast sedimentation.

During sunrise, fast resuspension prevails at lowest altitudes only for MAM and JJA, while other seasons show prevalent slow resuspension at lower levels. MAM exhibits slower resuspension with altitude, whereas JJA and SON show dominant slow sedimentation at the highest altitudes. DJF is characterized by dominant fast sedimentation with altitude.

During sunset, particle movement is considerably slower for MAM, JJA and SON, characterized by the dominance of slow sedimentation at all altitudes except the lowest, where slow resuspension dominates across all seasons. During DJF, strong dominance of fast sedimentation is observed at higher altitudes.

Nocturnal and residual layers exhibit the slowest particle motion for MAM JJA and SON, characterized predominantly by dominant slow sedimentation at all altitudes except the lowest, where slow resuspension only in MAM and DJF. For the DJF one can observe strong dominance of fast sedimentation only at high altitudes.

It should be noted that the high values observed during DJF may be influenced by chaotic variability resulting from small sample size due to limited aerosol signal availability (Fig. 9).

To synthesize the results and mitigate potential biases, such as the seasonal dominance of rapid sedimentation during winter (DJF), an aerosol flux intensity factor was introduced and applied. This factor is based on four variables: flux occurrence (1–4), transport prevalence (1–2), velocity regimes (1–4), and direction. Higher values in brackets correspond to an increased frequency of flux occurrence, transport direction prevalence, and velocity, respectively (as detailed in Fig. 6 and Fig. 11), resulting in a higher intensity factor. The final value of the factor is the product of the numbers in the brackets. Ultimately, a higher factor indicates a greater probability of significant resuspension or sedimentation. The aerosol flux intensity factor is shown in Fig. 12.

During daytime, strong and moderately intense resuspension dominates at lowest altitudes across all seasons. With increasing altitude, resuspension transitions to sedimentation or becomes less intense (as in MAM). In SON and DJF, less intense resuspension shifts to sedimentation at higher altitudes, while in JJA, strong resuspension transitions to moderately intense sedimentation before weakening at higher altitudes.

During nighttime across all seasons and altitudes, aerosol fluxes are relatively weak, particularly sedimentation, with resuspension occurring at the lowest altitudes only for MAM and DJF.

The WML is strongly dominated by intense resuspension, with the highest classified resuspension intensities occurring in MAM and JJA at the lowest altitudes, and in MAM also at higher altitudes. Intensified resuspension is also observed at lowest altitudes in SON and DJF. With increasing altitude, resuspension becomes less intense (in MAM) or transitioning to low-intensity sedimentation (in SON and DJF), while in JJA, strong resuspension shifts to moderately intense sedimentation before weakening at higher altitudes.

Sunrise exhibits very similar characteristics, but with decreased flux intensities while maintaining the same behaviour patterns. Only in DJF and SON the weak resuspension transitions to weak sedimentation at lower altitudes.

https://doi.org/10.5194/egusphere-2026-5029
Preprint. Discussion started: 27 August 2026

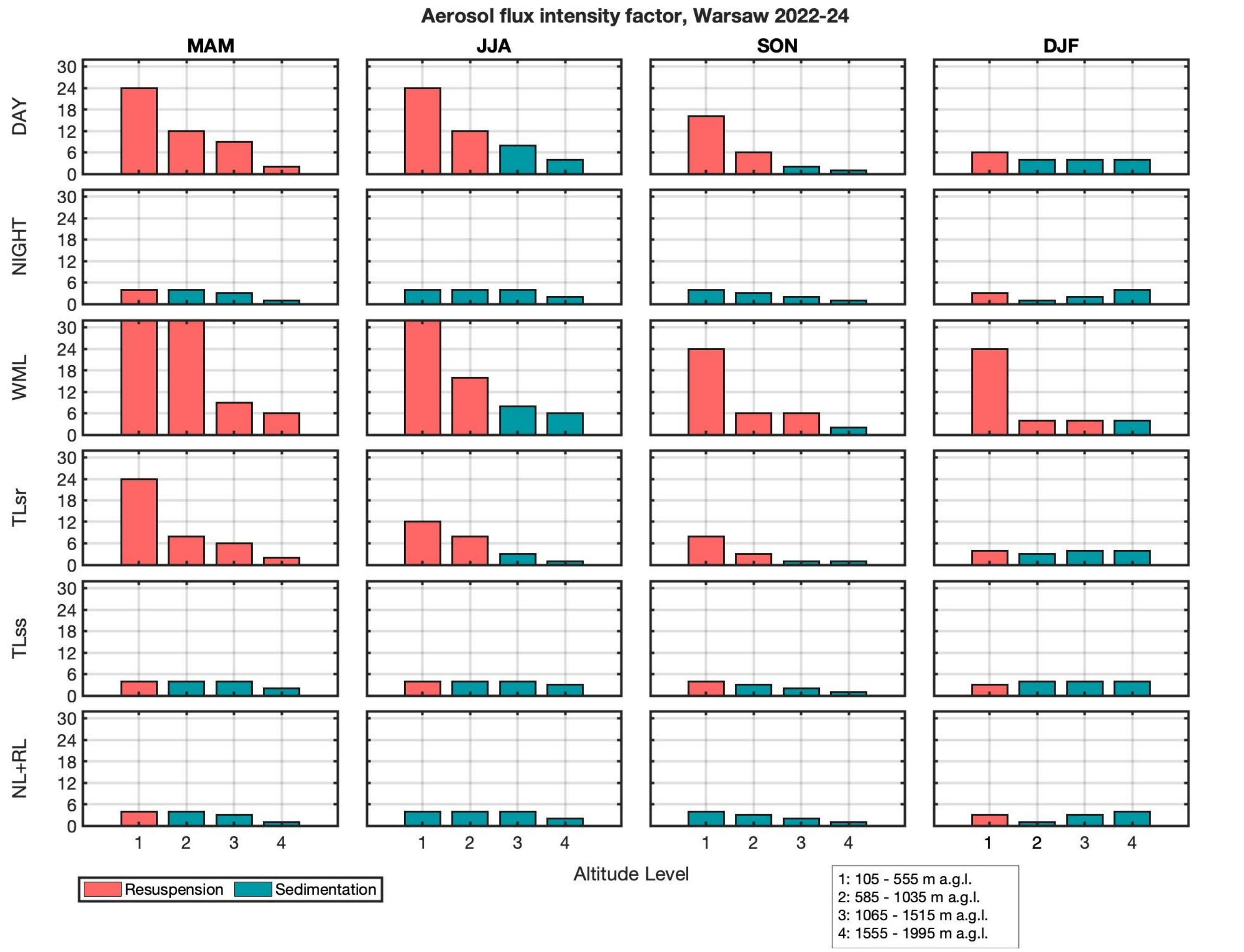

Figure 12. Normalized to 32 groups aerosol flux intensity factor. Numbers on the x-axis indicate the altitude levels. The rows names indicate the ABL sublayers and their time intervals according to Tab. 2.

During sunset, aerosol fluxes are relatively weaker across all seasons and altitudes, with weak sedimentation dominating at all altitudes except the lowest, where weak resuspension dominates.

A very similar situation occurs during nighttime, with weak sedimentation dominating across all altitudes and seasons, except at lowest altitudes in MAM and DJF where weak resuspension prevails.

6. Summary

Analysis of Doppler lidar - derived aerosol flux velocities during multi-seasonal observations for long-term measurements in urban environments, has been conducted. This work introduced the term „flux intensity” based on aerosol flux occurrence

https://doi.org/10.5194/egusphere-2026-5029
Preprint. Discussion started: 27 August 2026

frequency, transport direction predominance and dominance, and velocity regime according to predefined thresholds. The analysis reveals altitude, seasonal, and diurnal dependencies of aerosol flux velocities, categorizing their intensity using the introduced aerosol flux intensity factor. This represents the first comprehensive data analysis and characterization of vertical aerosol fluxes for an urban environment using multi-year (2022 -2024) Doppler lidar data in Warsaw, Poland.

The primary instrumentation consisted of a Doppler lidar system (StreamLine XR, HaloPhotonics) installed on the roof platform of Warsaw Observatory Station (WOS), an ACTRIS National Facility located at the Geophysics Institute, Faculty of Physics, University of Warsaw (IGF UW), along with co-located microwave radiometer (HATPRO-G2) and disdrometer (Parsivel^2 OTT HydroMet) have been used. Measurements were conducted within the Aerosol Cloud and Trace gases research infrastructure (ACTRIS-ERIC) and ACTRIS-PL as part of the Cloud Observations Network (Cloudnet-ACTRIS) routine observations.

Data from different seasons (Spring - MAM, Summer - JJA, Autumn - SON and Winter - DJF), for different stages of ABL transformation (Well Mixed Layer - WML, Transition layer during sunrise and sunset, respectively TLsr and TLss, and Nocturnal and Residual Layer - NL+RL) and for different altitude intervals (105 - 555, 585 - 1035, 1065 - 1515, 1555 - 1995 m a.g.l.) were analyzed. The results show that aerosol flux behavior in MAM and JJA is very similar during daytime at the lowest altitudes. However, they significantly differ at higher altitudes, where intensive sedimentation activity is noticeable in the JJA, while in the MAM, resuspension dominates and prevails at all altitudes. In this regard, JJA resembles SON in terms of resuspension occurrence at lower altitudes and sedimentation at higher altitudes, but with considerably more intense processes in JJA.

However, subtle changes in aerosol flux intensity can be observed from MAM, through JJA and SON to DJF, with a maximum intensity increase from DJF to MAM. Across all seasons, fluxes are most intense during WML and least intense during NL+RL. Similarities can be observed during ABL transformation, where TLsr resembles WML, characterized by a gradual flux activity increase to its relative diurnal maximum. Similar relationships exist between TLss and NL+RL. Rather than a gentle transition in flux intensity during the sunset, there is a sudden decrease of turbulent transport associated during rapid ABL decay. Nevertheless, resuspension characteristics are preserved at the lowest altitudes across all seasons during the sunset. While sedimentation processes occur as often as resuspension, resuspension processes are considerably more intense compared to the relatively weak sedimentation. However the most intense sedimentation is observed at higher altitudes during the JJA. Furthermore, maximum flux intensity does not strictly correlate with the maximum ABL height, although both show substantial increase between DJF and MAM, flux intensity peaks in MAM while ABLH peaks in JJA.

Our work presents a novel approach for data curation using the combined data products from multiple instruments, together with a methodology to classify aerosol fluxes based on their characteristics. We believe this work enables similar study across other Cloudnet-ACTRIS National Facilities and provides a solid foundation for multi-seasonal and multi-year flux intensity comparisons across Europe and globally. This work, as extended to all available data in the Cloudnet-ACTRIS database, will provide a solid basis for flux intensity comparisons across Europe, thereby significantly improving the accuracy of aerosol optical property assessments and providing a knowledge for aerosol vertical transport in the urban environment.

Data availability

The Doppler lidar, microwave radiometer and disdrometer data used in this study are generated by the Aerosol, Clouds and Trace Gases Research Infrastructure (ACTRIS) and are available from the Cloudnet-ACTRIS Data Centre using the following link: https://doi.org/10.60656/9c54c846af134629 (Doppler lidar), https://doi.org/10.60656/7d707b67335a4020 (microwave radiometer) and https://doi.org/10.60656/b7a8ac9413bd4cfc (disdrometer).
The Doppler lidar high-level data products (aerosol flux) were published in Repository for Open Data (RepOD) maintained by the Interdisciplinary Centre for Mathematical and Computational Modelling at the University of Warsaw, Poland (ICM UW): Karasewicz, Maciej; Janicka, Łucja; Ortiz-Amezca, Pablo; Kumala, Wojciech; Stachlewska, Iwona S., 2026, "Boundary layer aerosol flux: Doppler lidar dataset, Warsaw, Poland (2022-2024)", https://doi.org/10.18150/125DKQ, RepOD, V1 under the Creative Commons Zero 1.0 License.

Author contributions

MK: Writing - Original Draft, Methodology, Software, Formal Analysis, Investigation, Data curation, Visualization;
LJ: Writing - Review & Editing, Formal Analysis, Investigation, Validation;
RE: Writing - Review & Editing, Methodology, Validation;
LB: Writing - Review & Editing, Data Curation, Validation;
ISS: Writing - Original Draft, Conceptualization, Methodology, Investigation, Resources, Supervision, Project administration, Funding acquisition

Competing interests

Authors declare no conflict of interests

Acknowledgements

Authors would like to thank colleagues who contributed with software developments and technical assistance: Pablo Ortiz-Amezcua, Wojciech Kumala, Krzysztof Markowicz, Dongxiang Wang, Patryk Poczta and Igor Okraska.
Doppler lidar was purchased within investment funds of the Faculty of Physics, University of Warsaw. We are thankful for the provision of the disdrometer to IMGW-PIB (from polish: Instytut Meteorologii i Gospodarki Wodnej – Państwowy Instytut Badawczy, Poland) and the microwave radiometer to INOE 2000 (National Institute for Research and Development in Optoelectronics, Romania).
We acknowledge Cloudnet-ACTRIS and Finish Meteorological Institute for distributing our Doppler lidar, disdrometer and microwave radiometer datasets which are available for download from https://cloudnet.fmi.fi.

https://doi.org/10.5194/egusphere-2026-5029
Preprint. Discussion started: 27 August 2026

Financial support

The research has been financially supported by the European Space Agency (ESA-ESRIN) contact no. 4000142902/23/I-NS (AIRSENSE), the European Cooperation in Science and Technology, under the HARMONIA (International network for harmonization of atmospheric aerosol retrievals from ground-based photometers) COST Action CA21119 grant no. E-COST-GRANT-CA21119-5667ed2c (DLiAF), the European Commission Horizon 2020 Research and Innovation Programme grants no. 871115 (ACTRIS-IMP), 101008004 (ATMO-ACCESS), 101132093 (CARGO-ACT), the Ministry of Science and Higher Education (Poland) under the programme 'Support for the participation of Polish scientific teams in international research infrastructure projects' grant no. 2024/WK/04 (ACTRIS-ERIC Poland), the Romanian National Research Development and Innovation Plan 2022-2027, project no. PN 23-05 and Smart Growth and Digitization and Financial Instruments Program - PoCIDIF 2021-2027, project "Supporting the operation of facilities in Romania within the ACTRIS ERIC research infrastructure", SMIS code 309113 (ACTRIS-ERIC Romania).

Review statement

The review statement will be added by Copernicus Publications listing the handling editor as well as all contributing referees according to their status anonymous or identified.

References

Abril-Gago, J., Ortiz-Amezcua, P., Kowalski, A., S., Bravo-Aranda, J., A., Granados-Muñoz, M., J., Andújar-Maqueda, J., Alados-Arboledas, L., Guerrero-Rascado, J., L. (2025). Quantifying turbulent coarse particle transport over drylands of Southeastern Iberia using a stand-alone Doppler lidar methodology, Atmospheric Research, Volume 325, 2025, 108236, ISSN 0169-8095, https://doi.org/10.1016/j.atmosres.2025.108236.

Baars, H., Seifert, P., Engelmann, R., and Wandinger, U. (2017) Target categorization of aerosol and clouds by continuous multiwavelength-polarization lidar measurements, Atmos. Meas. Tech., 10, 3175–3201, https://doi.org/10.5194/amt-10-3175-2017, 2017.

Chinchella, E., Cauteruccio, A., & Lanza, L. G. (2025). Impact of Wind on Rainfall Measurements Obtained from the OTT Parsivel^2 Disdrometer. Sensors, 25(20), 6440. https://doi.org/10.3390/s25206440

Chen, B., Dong, L., Huang, J., Wang, Y., Jing, Z., Yan, W., et al. (2023). Analysis of long-term trends in the vertical distribution and transport paths of atmospheric aerosols in typical regions of China using 15 years of CALIOP data. Journal of Geophysical Research: Atmospheres, 128, e2022JD038066. https://doi.org/10.1029/2022JD038066

https://doi.org/10.5194/egusphere-2026-5029
Preprint. Discussion started: 27 August 2026

Chen, L., Peng, C., Gu, W., Fu, H., Jian, X., Zhang, H., Zhang, G., Zhu, J., Wang, X., and Tang, M.: On mineral dust aerosol hygroscopicity, Atmos. Chem. Phys., 20, 13611–13626, https://doi.org/10.5194/acp-20-13611-2020, 2020.

Chung, C. E., V. Ramanathan, D. Kim, and I. A. Podgorny (2005). Global anthropogenic aerosol direct forcing derived from satellite and ground-based observations, J. Geophys. Res., 110, D24207, doi:10.1029/2005JD006356

Coakley, J. A., R. D. Cess, and F. B. Yurevich, (1983). The Effect of Tropospheric Aerosols on the Earth's Radiation Budget: A Parameterization for Climate Models. J. Atmos. Sci., 40, 116–138, https://doi.org/10.1175/1520-0469(1983)040<0116:TEOTAO>2.0.CO;2.

Dai, G., X. Wang, K. Sun, S. Wu, X. Song, R. Li, J. Yin, and X. Wang, (2021). Calibration and Retrieval of Aerosol Optical Properties Measured with Coherent Doppler Lidar. J. Atmos. Oceanic Technol., 38, 1035–1045, https://doi.org/10.1175/JTECH-D-20-0190.1.

Engelmann, R., Wandinger, U., Ansmann, A., Müller, D., Žeromskis, E., Althausen, D., & Wehner, B. (2008). Lidar observations of the vertical aerosol flux in the planetary boundary layer. Journal of Atmospheric and Oceanic Technology, 25, 1296–1306. https://doi.org/10.1175/2007JTECHA967.1

Fridlind, et al. (2004). Evidence for the predominance of mid-tropospheric aerosols as subtropical anvil cloud nuclei. Science, 304, 718–722. https://doi.org/10.1126/science.1094947

Fragkos, K., Antonescu, B., Giles, D. M., Ene, D., Boldeanu, M., Efstathiou, G. A., Belegante, L., and Nicolae, D. (2019). Assessment of the total precipitable water from a sun photometer, microwave radiometer and radiosondes at a continental site in southeastern Europe, Atmos. Meas. Tech., 12, 1979–1997, https://doi.org/10.5194/amt-12-1979-2019, 2019.

Gui, L., Tao, M., Wang, Y., Wang, L., Chen, L., Lin, C., Tao, J., Wang, J., & Yu, C. (2022). Climatology of aerosol types and their vertical distribution over East Asia based on CALIPSO lidar measurements. International Journal of Climatology, 42(11), 6042–6054. https://doi.org/10.1002/joc.7599

Guo, J., Liu, H., Li, Z., Rosenfeld, D., Jiang, M., Xu, W., Jiang, J. H., He, J., Chen, D., Min, M., and Zhai, P. (2018). Aerosol-induced changes in the vertical structure of precipitation: a perspective of TRMM precipitation radar, Atmos. Chem. Phys., 18, 13329–13343, https://doi.org/10.5194/acp-18-13329-2018, 2018.

Haywood, J., & Boucher, O. (2000). Estimates of the direct and indirect radiative forcing due to tropospheric aerosols: A review. Reviews of Geophysics, 38(4), 513–543. https://doi.org/10.1029/1999RG000078

IPCC. (2021). Climate Change 2021: The Physical Science Basis. Cambridge University Press. https://doi.org/10.1017/9781009157896

https://doi.org/10.5194/egusphere-2026-5029
Preprint. Discussion started: 27 August 2026

IPCC. (2023). Climate Change 2023: Synthesis Report. IPCC, Geneva. https://doi.org/10.59327/IPCC/AR6-9789291691647

Janicka, L., Stachlewska, I. S., Veselovskii, I., Baars, H. (2017). Temporal variations in optical and microphysical properties of mineral dust and biomass burning aerosol derived from daytime Raman lidar observations over Warsaw, Poland, Atmospheric Environment, Volume 169, 2017, Pages 162-174, ISSN 1352-2310, https://doi.org/10.1016/j.atmosenv.2017.09.022.

Janicka, L., Davuliene L., Bycenkiene S., and Stachlewska I., S. (2023). Long term observations of biomass burning aerosol over Warsaw by means of multiwavelength lidar, Opt. Express 31, 33150-33174 (2023). https://opg.optica.org/oe/fulltext.cfm?uri=oe-31-20-33150

Janicka, L., and Stachlewska, I. S. (2026). Custom collection of disdrometer data from Warsaw between 1 Jan 2022 and 31 Dec 2024. ACTRIS Cloud remote sensing data centre unit (CLU). https://doi.org/10.60656/a1a0a07044b54134

Järvi, L., Rannik, Ü., Mammarella, I., Sogachev, A., Aalto, P. P., Keronen, P., Siivola, E., Kulmala, M., and Vesala, T. (2009). Annual particle flux observations over a heterogeneous urban area, Atmos. Chem. Phys., 9, 7847–7856, https://doi.org/10.5194/acp-9-7847-2009, 2009.

Ji, D., Palm, M., Buschmann, M., Ebell, K., Maturilli, M., Sun, X., & Notholt, J. (2025). Hygroscopic aerosols amplify longwave downward radiation in the Arctic. Atmospheric Chemistry and Physics, 25, 3889–3904. https://doi.org/10.5194/acp-25-3889-2025

Karasewicz, M., Wacławczyk, M., Ortiz-Amezcua, P., Janicka, Ł., Poczta, P., Kassar Borges, C., and Stachlewska, I. S. (2024). Investigation of non-equilibrium turbulence decay in the atmospheric boundary layer using Doppler lidar measurements. Atmospheric Chemistry and Physics, 24, 13231–13251. https://doi.org/10.5194/acp-24-13231-2024

Karasewicz, M., Janicka, L., and Stachlewska, I. S. (2026). Custom collection of Doppler lidar data from Warsaw between 1 Jan 2022 and 31 Dec 2024. ACTRIS Cloud remote sensing data centre unit (CLU). https://doi.org/10.60656/9c54c846af134629

Karasewicz, M., Janicka, L., Ortiz-Amezca, P., Kumala, W., Stachlewska, I. S., (2026). Boundary layer aerosol flux: Doppler lidar dataset, Warsaw, Poland (2022-2024), https://doi.org/10.18150/125DKQ, RepOD, V1

Kumala, W., Karasewicz, M., Stachlewska, I. S., & Janicka, Ł. (2026). Custom collection of MWR multiple pointing data from Warsaw between 10 Jan 2022 and 31 Dec 2024. ACTRIS Cloud remote sensing data centre unit (CLU). https://doi.org/10.60656/7d707b67335a4020

https://doi.org/10.5194/egusphere-2026-5029
Preprint. Discussion started: 27 August 2026

Kim, G., Lee, J., Lee, M.-I., & Kim, D. (2021). Impacts of urbanization on atmospheric circulation and aerosol transport in a coastal environment simulated by the WRF-Chem coupled with urban canopy model. Atmospheric Environment, 249, 118253. https://doi.org/10.1016/j.atmosenv.2021.118253

Kuang, Y., Zhao, C. S., Ma, N., Liu, H. J., Bian, Y. X., Tao, J. C., & Hu, M. (2016). Deliquescent phenomena of ambient aerosols on the North China Plain. Geophysical Research Letters, 43, 8744–8750. https://doi.org/10.1002/2016GL070273

Labzovskii, L. D., Papayannis, A., Binietoglou, I., Banks, R. F., Baldasano, J. M., Toanca, F., Tzanis, C. G., and Christodoulakis, J. (2018). Relative humidity vertical profiling using lidar-based synergistic methods in the framework of the Hygra-CD campaign, Ann. Geophys., 36, 213–229, https://doi.org/10.5194/angeo-36-213-2018, 2018.

Liu, X., Zhang, Y., Cheng, Y., Hu, M., Han T. (2012). Aerosol hygroscopicity and its impact on atmospheric visibility and radiative forcing in Guangzhou during the 2006 PRIDE-PRD campaign, Atmospheric Environment, Volume 60, 2012, Pages 59-67, ISSN 1352-2310, https://doi.org/10.1016/j.atmosenv.2012.06.016.

Manninen, A. J., O'Connor, E. J., Vakkari, V., and Petäjä, T. (2016) A generalised background correction algorithm for a Halo Doppler lidar and its application to data from Finland, Atmos. Meas. Tech., 9, 817–827, https://doi.org/10.5194/amt-9-817-2016, 2016.

Manninen, A. J., Marke, T., Tuononen, M. J., & O'Connor, E. J. (2018). Atmospheric boundary layer classification with Doppler lidar. Journal of Geophysical Research: Atmospheres, 123, 8172–8189. https://doi.org/10.1029/2017JD028169

Mishra, A., K., Shibata, T. (2022). Climatological aspects of seasonal variation of aerosol vertical distribution over central Indo-Gangetic belt (IGB) inferred by the space-borne lidar CALIOP, Atmospheric Environment, Volume 46, 2012, Pages 365-375, ISSN 1352-2310, https://doi.org/10.1016/j.atmosenv.2011.09.052.

Ortiz-Amezcua, P. (2023). Remote Sensing Aerosol Flux Toolbox. Zenodo. https://doi.org/10.5281/zenodo.8394916

Pearson, G., F. Davies, and C. Collier (2009). An Analysis of the Performance of the UFAM Pulsed Doppler Lidar for Observing the Boundary Layer. J. Atmos. Oceanic Technol., 26, 240–250, https://doi.org/10.1175/2008JTECHA1128.1.

Rose, T., Crewell, S., Löhnert, U., Simmer, C. (2005). A network suitable microwave radiometer for operational monitoring of the cloudy atmosphere, Atmospheric Research, Volume 75, Issue 3, 2005, Pages 183-200, ISSN 0169-8095, https://doi.org/10.1016/j.atmosres.2004.12.005.

Sorbjan, Z. (1989). Structure of the Atmospheric Boundary Layer. Prentice Hall, Englewood Cliffs, NJ, USA.

https://doi.org/10.5194/egusphere-2026-5029
Preprint. Discussion started: 27 August 2026

Stull, R. B. (1988). An Introduction to Boundary Layer Meteorology. Kluwer Academic Publishers. https://doi.org/10.1007/978-94-009-3027-8

Sun, X., Zhou, Y., Zhao, T., Fu, W., Wang, Z., Shi, C., Zhang, H., Zhang, Y., Yang, Q., Shu, Z. (2024). Vertical distribution of aerosols and association with atmospheric boundary layer structures during regional aerosol transport over central China. Environmental Pollution. https://doi.org/10.1016/j.envpol.2024.124967

Szczepanik, D., M., Poczta P., Talianu C., Böckmann C., Ritter C., Stefanie H., Toanca, F., Chojnicki, B., H., Schüttemeyer, D., Stachlewska, I., S., (2023). Spatio-temporal evolution of long-range transported mineral desert dust properties over rural and urban sites in Central Europe, Science of The Total Environment, Volume 903, 2023, 166173, ISSN 0048-9697, https://doi.org/10.1016/j.scitotenv.2023.166173.

Tang, M., Gu, W., Ma, Q., Li, Y. J., Zhong, C., Li, S., Yin, X., Huang, R.-J., He, H., and Wang, X. (2019). Water adsorption and hygroscopic growth of six anemophilous pollen species: the effect of temperature, Atmos. Chem. Phys., 19, 2247–2258, https://doi.org/10.5194/acp-19-2247-2019, 2019.

Tian, P., Cao, X., Zhang, L., Sun, N., Sun, L., Logan, T., Shi, J., Wang, Y., Ji, Y., Lin, Y., Huang, Z., Zhou, T., Shi, Y., and Zhang, R. (2017). Aerosol vertical distribution and optical properties over China from long-term satellite and ground-based remote sensing, Atmos. Chem. Phys., 17, 2509–2523, https://doi.org/10.5194/acp-17-2509-2017, 2017.

Twomey, S., (1977). The Influence of Pollution on the Shortwave Albedo of Clouds. J. Atmos. Sci., 34, 1149–1152, https://doi.org/10.1175/1520-0469(1977)034<1149:TIOPOT>2.0.CO;2.

Vakkari, V., Manninen, A. J., O'Connor, E. J., Schween, J. H., van Zyl, P. G., and Marinou, E. (2019). A novel post-processing algorithm for Halo Doppler lidars, Atmos. Meas. Tech., 12, 839–852, https://doi.org/10.5194/amt-12-839-2019, 2019.

Wang, D., Stachlewska, I., S., Delanoë, J., Ene, D., Song, X., and Schüttemeyer D. (2020a). Spatio-temporal discrimination of molecular, aerosol and cloud scattering and polarization using a combination of a Raman lidar, Doppler cloud radar and microwave radiometer, Opt. Express 28, 20117-20134 (2020a). https://doi.org/10.1364/OE.393625

Wang, D., Stachlewska, I. S., Song, X., Heese, B., & Nemuc, A. (2020b). Variability of the boundary layer over an urban continental site based on 10 years of active remote sensing observations in Warsaw. Remote Sensing, 12, 340. https://doi.org/10.3390/rs12020340

Wang, H., Sun, Z., Li, H., Gao, Y., Wu, J., & Cheng, T. (2018). Vertical-distribution characteristics of atmospheric aerosols under different thermodynamic conditions in Beijing. Aerosol and Air Quality Research, 18, 2775–2787. https://doi.org/10.4209/aaqr.2018.03.0078

https://doi.org/10.5194/egusphere-2026-5029
Preprint. Discussion started: 27 August 2026

Wonaschütz, A., Coggon, M., Sorooshian, A., Modini, R., Frossard, A. A., Ahlm, L., Mülmenstädt, J., Roberts, G. C., Russell, L. M., Dey, S., Brechtel, F. J., and Seinfeld, J. H. (2013) Hygroscopic properties of smoke-generated organic aerosol particles emitted in the marine atmosphere, Atmos. Chem. Phys., 13, 9819–9835, https://doi.org/10.5194/acp-13-9819-2013, 2013.

Wu, Y., Wang, X., Yan, P., Zhang, L., Tao, J., Liu, X., Tian, P., Han, Z., Zhang R. (2017). Investigation of hygroscopic growth effect on aerosol scattering coefficient at a rural site in the southern North China Plain, Science of The Total Environment, Volumes 599–600, 2017, Pages 76-84, ISSN 0048-9697, https://doi.org/10.1016/j.scitotenv.2017.04.194.

Yang, Y., Zheng, Z., Yim, S. Y. L., Roth, M., Ren, G., Gao, Z., et al. (2020). PM2.5 pollution modulates wintertime urban heat island intensity in the Beijing-Tianjin-Hebei Megalopolis, China. Geophysical Research Letters, 47, e2019GL084288. https://doi.org/10.1029/2019GL084288